

# Infrared Spectroscopy of Quantum Crossbars

I. Kuzmenko<sup>1</sup>, S. Gredeskul<sup>1</sup>, K. Kikoin<sup>1</sup>, Y. Avishai<sup>1,2</sup>

<sup>1</sup>*Department of Physics,*

<sup>2</sup>*The Ilse Katz Center for Mezo and Nanoscale Science and Technology,  
Ben-Gurion University of the Negev, Beer-Sheva*

(November 13, 2018)

Infrared (IR) spectroscopy can be used as an important and effective tool for probing periodic networks of quantum wires or nanotubes (quantum crossbars, QCB) at finite frequencies far from the Luttinger liquid fixed point. Plasmon excitations in QCB may be involved in resonance diffraction of incident electromagnetic waves and in optical absorption in the IR part of the spectrum. Direct absorption of external electric field in QCB strongly depends on the direction of the wave vector  $\mathbf{q}$ . This results in two types of  $1D \rightarrow 2D$  dimensional crossover with varying angle of an incident wave or its frequency. In the case of QCB interacting with semiconductor substrate, capacitive contact between them does not destroy the Luttinger liquid character of the long wave QCB excitations. However, the dielectric losses on a substrate surface are significantly changed due to appearance of additional Landau damping. The latter is initiated by diffraction processes on QCB superlattice and manifests itself as strong but narrow absorption peaks lying below the damping region of an isolated substrate.

PACS 73.90.+f;74.22.Gm;78.67.Pt

## I. INTRODUCTION

Recent achievements in material science and technology have led to creation of an unprecedented variety of artificial structures that possess properties never encountered in "natural" quantum objects. One of the most exciting developments in this field is fabrication of two-dimensional (2D) networks by means of self-assembling, etching, lithography and imprinting techniques<sup>1,2</sup>. Another development is the construction of 2D molecular electronic circuits<sup>3</sup> where the network is formed by chemically assembled molecular chains. Such networks have the geometry of crossbars, and bistable conformations of molecular chain may be used as logical elements<sup>4</sup>. Especially remarkable is a recent experimental proposal to fabricate 2D periodic grids from single-wall carbon nanotubes (SWCNT) suspended above a dielectric substrate<sup>5</sup>. The possibility of excitation of a SWCNT by external electric field together with its mechanical flexibility makes such a grid formed by nanotubes a good candidate for an element of random access memory for molecular computing.

From a theoretical point of view, such double 2D grid i.e. two superimposed crossing arrays of parallel conducting quantum wires<sup>6-8</sup> or nanotubes<sup>9</sup>, represent a unique nano-object - quantum crossbars (QCB). Its spectral properties can not be treated in terms of purely 1D or 2D electron liquid theory. A constituent element of QCB (quantum wire or nanotube) possesses the Luttinger liquid (LL) like spectrum<sup>10,11</sup>. A single array of parallel quantum wires is still a LL-like system qualified as a sliding phase<sup>9</sup> provided only the electrostatic interaction between adjacent wires is taken into account. If an inter-wire tunneling is possible, the electronic spectrum of an array is that of 2D Fermi liquid (FL)<sup>12,13</sup>.

Similar low-energy, long-wave properties are characteristic of QCB as well. Its phase diagram inherits some properties of a sliding phases in case when the wires and arrays are coupled only by capacitive interaction<sup>9,14</sup>. When inter-array electron tunneling is possible, say, in crosses, dimensional crossover from LL to 2D FL occurs<sup>15,9,16</sup>. If tunneling is suppressed and the two arrays are coupled only by electrostatic interaction in the crosses, the system possesses the LL zero energy fixed point, and a rich Bose-type excitation spectrum (plasmon modes) arises at finite energies in 2D Brillouin zone (BZ)<sup>14,19</sup>. These QCB plasmons can be treated as a set of dipoles distributed within QCB constituents. In a single wire the density of the dipole momentum is proportional to the LL boson field  $\theta(x)$  ( $x$  is the coordinate along the wire).

Two sets of coupled 1D dipoles form unique system which possesses the properties of 1D and 2D liquid depending on the type of experimental probe. Some possibilities of observation of  $1D \rightarrow 2D$  crossover in transport measurements were discussed in Ref. 9. Here we consider various possibilities of direct observation of plasmon spectra at finite frequencies and wave vectors by the methods of IR spectroscopy.

In transport measurements, the geometrical factors regulate the crossover from anisotropic to isotropic resistivity of QCB: one may study the dc response for a field applied either parallel to one of the constituent arrays or in arbitrary direction. One may also study spatially nonuniform response by means of two probes inserted at different points of QCB and regulate the length scale i.e. the distance between two probes in comparison with the periods of the crossbar superlattice. These methods give information about nearest vicinity of LL fixed point at  $(q, \omega, T) \rightarrow 0$ .

Unlike transport measurements, the methods of in-

frared spectroscopy provide an effective tool for investigating the excitation spectrum in wide enough  $(q, \omega)$  area well beyond the sliding phase region. We will show that the IR spectroscopy allows scanning of  $2D$  Brillouin zone in various directions and thereby elucidates dimensional crossover in the high symmetry points of the BZ.

Several crossover effects such as appearance of non-zero transverse space correlators and periodic energy transfer between arrays ("Rabi oscillations") were discussed in our earlier publications<sup>17,18</sup>. The direct manifestation of dimensional crossover is the response to an external ac electromagnetic field. To estimate this response one should note that the two main parameters characterising the plasmon spectrum in QCB are the Fermi velocity  $v$  of electrons in a wire and the QCB period  $a$  (we assume both periods to be equal). These parameters define both the typical QCB plasmon wave numbers  $q = |\mathbf{q}| \sim Q = 2\pi/a$  and the typical plasmon frequencies  $\omega \sim \omega_Q = vQ$ . Choosing according to Refs.[ 11, 5]  $v \approx 0.8 \cdot 10^6$  m/sec and  $a \approx 20$  nm, one finds that characteristic plasmon frequencies lie in the far infrared region  $\omega \sim 10^{14}$  sec<sup>-1</sup>, while characteristic wave vectors are estimated as  $q \sim 10^6$  cm<sup>-1</sup>.

In this paper we study high frequency properties of the simplest double square QCB (generalization to more complicated geometries is straightforward). We start from QCB interacting with an external infrared radiation. The plasmon velocity  $v$  is much smaller than the light velocity  $c$  and the light wave vector  $k$  is three orders of magnitude smaller than the characteristic plasmon wave vector  $Q$  corresponding to the same frequency. Therefore, infrared radiation incident directly on an *isolated* array, can not excite plasmons at all (it could excite plasmon with  $\omega \neq 0$ ). However in QCB geometry, each array serves as a diffraction lattice for its partner, giving rise to Umklapp processes of wave vectors  $nQ$ ,  $n$  integer. As a result, excitation of plasmons in the BZ center  $q = 0$  with frequencies  $nvQ$  occurs.

To excite QCB plasmons with  $q \neq 0$  one may use an additional diffraction lattice (DL) with period  $A > a$  coplanar to the QCB. Here the diffraction field contains space harmonics with wave vectors  $2\pi M/A$ ,  $M$  integer, that enables one to scan plasmon spectrum within the BZ. Dimensional crossover manifests itself in the appearance of additional absorption lines when the wave vector of diffraction field is oriented along specific directions. In the general case one observes the single absorption lines forming two sets of equidistant series. Instead of that, in the main resonance direction (QCB diagonal) an equidistant series of split doublets can be observed. In the case of higher resonance direction, absorption lines form an alternating series of singlets and split doublets demonstrating new type of dimensional crossover related to the frequency change with direction fixed.

We study also QCB interacting with a semiconducting substrate. This interaction may be rather strong because

surface plasmon waves exist in the same frequency and wave vector area as plasmons in QCB. This problem is interesting from at least two points of view. First, technological reasons may lead to creation of QCB embedded into thin layer of semiconductor medium. Second, the question of stability of LL regime in QCB against interaction with  $2D$  plasmons in substrate, is itself of great interest. It will be shown that in spite of the long range character of 2D screening, the substrate plasmons only renormalize the velocity of the QCB plasmons and do not destroy LL character of the QCB spectrum. At the same time, QCB-substrate resonance can be observed experimentally in special directions. Moreover, at a special frequency, a triple resonance involving both QCB modes and substrate plasmons is possible.

The structure of the paper is as follows. In section II, we briefly describe double square QCB and introduce the necessary definitions. Interaction of QCB with external field is studied in section III. In its first part we consider the case when the incident infrared radiation falls directly on the QCB (subsection III A). In the second part III B we study possible scanning of QCB spectrum with the help of an external DL. Dielectric properties of a combined system QCB-substrate are studied in the last section IV. In the Conclusion we summarize the results obtained.

## II. DOUBLE SQUARE QCB

A square QCB is a  $2D$  grid, formed by two periodically crossed perpendicular arrays of  $1D$  quantum wires or carbon nanotubes. Arrays are labeled by indices  $j = 1, 2$  and wires within the first (second) array are labeled by an integer index  $n_2$  ( $n_1$ ). In experimentally realizable setups, QCB is a cross-structure of suspended single-wall carbon nanotubes lying in two parallel planes separated by an inter-plane distance  $d$ , placed on a dielectric or semiconducting substrate (see Fig.1). Nevertheless, some generic properties of QCB may be described under the assumption that QCB is a genuine  $2D$  system. We choose coordinate system so that 1) the axes  $x_j$  and corresponding basic unit vectors  $\mathbf{e}_j$  are oriented along the  $j$ -th array; 2) the  $x_3$  axis is perpendicular to QCB plane; 3)  $x_3$  coordinate is zero for the second array,  $-d$  for the first one, and  $-(d + D)$  for the substrate. The basic vectors of the reciprocal superlattice for a square QCB are  $Q\mathbf{e}_{1,2}$ ,  $Q = 2\pi/a$  so that an arbitrary reciprocal superlattice vector  $\mathbf{m}$  is a sum  $\mathbf{m} = \mathbf{m}_1 + \mathbf{m}_2$ , where  $\mathbf{m}_j = m_j Q\mathbf{e}_j$ , ( $m_j$  integer). The first BZ is a square  $|q_{1,2}| \leq Q/2$ .

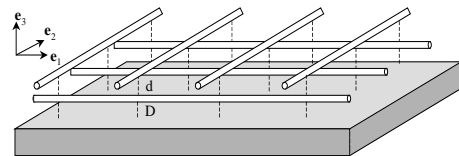


FIG. 1. QCB on a substrate.  $\mathbf{e}_j$  - basic vectors of the coordinate system. Vector  $\mathbf{e}_1$  ( $\mathbf{e}_2$ ) is oriented along the first (second) array. The inter-array distance is  $d$  and the distance between substrate and the first (lower) array is  $D$ .

A single wire is characterized by its radius  $r_0$ , length  $L$ , and LL interaction parameter  $g$ . The minimal nanotube radius is  $r_0 \approx 0.35$  nm<sup>20</sup>, maximal nanotube length is  $L \approx 1$  mm, and the LL parameter is estimated as  $g \approx 0.3$ <sup>11</sup>. In typical experimental setup<sup>5</sup> the characteristic lengths mentioned above have the following values

$$d \approx 2 \text{ nm}, \quad L \approx 0.1 \text{ mm},$$

so that the inequalities

$$r_0 \ll d \ll a \ll L$$

are satisfied.

The Hamiltonian of QCB interacting with an external field is

$$H = H_{QCB} + H_E. \quad (1)$$

The QCB interaction  $H_E$  with an external electric field  $\mathbf{E} = (E_1, E_2, E_3)$  is nothing but an energy of a set of QCB dipoles in this field

$$H_E = -e\sqrt{2} \left\{ \sum_{n_2} \int dx_1 E_1(x_1, n_2a, -d) \theta_1(x_1, n_2a, -d) + \sum_{n_1} \int dx_2 E_2(n_1a, x_2, 0) \theta_2(n_1a, x_2, 0) \right\}$$

where  $\theta_j$  is one of the two conventional canonically conjugate boson fields  $\pi_j, \theta_j$ .

The QCB Hamiltonian

$$H_{QCB} = H_1 + H_2 + H_{12}. \quad (2)$$

consists of three terms. The first of them describes LL in the first array

$$H_1 = \frac{\hbar v}{2} \sum_{n_2} \int_{-L/2}^{L/2} dx_1 \left\{ g\pi_1^2(x_1, n_2a, -d) + \frac{1}{g} (\partial_{x_1} \theta_1(x_1, n_2a, -d))^2 \right\}.$$

The Hamiltonian  $H_2$  is obtained from  $H_1$  after permutation  $1 \leftrightarrow 2$  and replacement  $-d \rightarrow 0$  in the arguments of the fields.

The inter-array interaction is described by the last term in Eq.(2)

$$H_{12} = V_0 \sum_{n_1, n_2} \int dx_1 dx_2 \zeta \left( \frac{x_1 - n_1a}{r_0} \right) \zeta \left( \frac{n_2a - x_2}{r_0} \right) \times \partial_{x_1} \theta_1(x_1, n_2a, -d) \partial_{x_2} \theta_2(n_1a, x_2, 0), \quad V_0 = \frac{2e^2}{d}. \quad (3)$$

It results from a short-range contact capacitive coupling in the crosses of the bars. The dimensionless envelope function (introduced phenomenologically)  $\zeta(\tau_j)$  describes re-distribution of a charge in a tube  $j$  induced by the interaction with tube  $i$ . This function is of order unity for  $|\tau| \sim 1$  and vanishes outside this region so that the dimensionless integral

$$\int \zeta(\tau) e^{ikr_0\tau} d\tau \sim 1$$

is of order unity for all  $|k|$  smaller than a certain ultraviolet cutoff. For simplicity, we put it equal to unity in what follows.

Before turning to investigation of QCB interaction with an external field, we briefly describe the spectral properties of the QCB itself<sup>18</sup>. The QCB Hamiltonian (2) is a quadratic form in terms of the field operators, so it can be diagonalized exactly. Such a procedure is rather cumbersome. However, due to the separability of the interaction (3) the spectrum can be described analytically. Moreover, being small, this interaction grossly conserves the unperturbed 1D systematics of levels and states, at least in the low energy region corresponding to the first few energy bands. This means that perturbed eigenstates could be described in terms of the same quantum numbers (array number, band number and quasimomentum) as the unperturbed eigenstates of an “empty” lattice. Such a description fails in two specific regions of a reciprocal space  $\mathbf{k} = k_1\mathbf{e}_1 + k_2\mathbf{e}_2$ . The first of them is the vicinity of high symmetry lines  $k_j = nQ/2$  with  $n$  integer (the lines with  $n = \pm 1$  include BZ boundaries). Around these lines, the *interband* mixing is significant and two modes from the adjacent bands are degenerate. The second region is the vicinity of the resonant lines  $k_1 \pm k_2 = nQ$  where the eigenfrequencies of unperturbed plasmons from the same band  $s$  propagating along two arrays coincide  $\omega_{1s}(q_1) = \omega_{2s}(q_2)$ . Around resonant lines *inter-array* mixing is significant and at these lines two modes corresponding to different arrays are degenerate.

Inter-array interaction introduces real two dimensionality into the problem, lifts the degeneracy of bare modes and splits degenerate frequencies. Therefore the simplest way to probe 2D nature of QCB is to observe this splitting in the corresponding spectral region. Possible ways of such an observation are discussed in the next two sections.

### III. INFRARED LIGHT ABSORPTION BY QCB

#### A. Long Wave Absorption

In the case of a dielectric substrate transparent in the infrared region, one can treat QCB as an isolated grid (without substrate) interacting directly with the incident radiation. Consider the simplest geometry (see Fig.2 for

details) where an external wave falls normally onto QCB plane, and its electrical field

$$\mathbf{E} = E_0 \mathbf{e}_1 \cos(\mathbf{k}\mathbf{r} - \omega t)$$

is parallel to the lower (first) array. In this geometry the field  $\mathbf{E}$  is *longitudinal* for array 1 and *transverse* for the array 2. The eigenfrequencies of transverse modes in array 2 substantially exceed the IR frequency of the incident wave and even the standard LL ultraviolet cut-off frequency. Thus, the incident wave can be treated as a static polarization field for this array, and the factor  $\cos \omega t$  can be omitted. Then, the polarization waves in array 2 form a longitudinal diffraction field for array 1 with quasi wave vectors  $nQ$  ( $n$  integer). Further, the characteristic order of magnitude  $Q$  of a QCB plasmon wave vector is much larger than the wave vector  $\mathbf{k}$  of the incident light, and we put the latter equal to zero from the very beginning. Then, the light wavelength is much larger than a nanotube diameter and the geometrical shadow effect can be neglected. As a result the total field which affects array 1 consists of an external field and a diffraction field produced by a static charge induced in array 2.

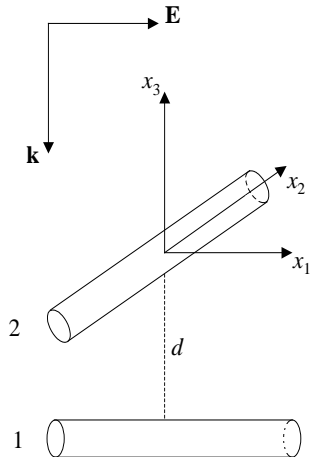


FIG. 2. The incident field orientation with respect to QCB. The axes  $x_1$  and  $x_2$  are directed along the corresponding arrays, and  $d$  is the inter-array vertical distance (along the  $x_3$  axis).

To calculate diffraction field consider first the field  $\mathbf{E}^0$  produced by the quantum wire of array 2 which is located at  $x_1 = x_3 = 0$  and labeled by  $n_1 = 0$ . The large distance between the wire under consideration and its neighbour partners from the same array allows us to neglect the influence of the charges induced on them. The static potential on the surface of the wire includes external potential of an incident field and the potential  $\Phi^0$  of the charge induced on the wire. On the other hand this static potential should be equal to a constant which we choose to be zero. In cylindrical coordinates  $r, \vartheta, x_2$ ,  $x_1 = r \cos \vartheta, x_3 = r \sin \vartheta$ , this condition reads

$$\Phi^0(R_0, \vartheta, x_2) = E_0 r_0 \cos \vartheta. \quad (4)$$

Outside the wire, induced potential  $\Phi^0$  satisfies Laplace equation  $\Delta \Phi^0 = 0$ . Solving this equation with boundary

condition (4) we obtain the static part of the induced potential

$$\Phi^0(r, \vartheta, x_2) = \frac{E_0 r_0^2}{r} \cos \vartheta$$

and the corresponding static part of the induced field along  $x_1$  direction

$$E_1^0(x_1, x_3) = -E_0 \frac{r_0^2 (x_3^2 - x_1^2)}{(x_3^2 + x_1^2)^2}.$$

The first component of the diffraction field is the sum of the fields induced by all wires of the upper array,

$$\begin{aligned} E_1(x_1; t) &= \cos \omega t \sum_{n_1} E_1^0(x_1 - n_1 a, -d) \\ &= -E_0 \cos \omega t \sum_{n_1} \frac{r_0^2 (d^2 - (x_1 - n_1 a)^2)}{(d^2 + (x_1 - n_1 a)^2)^2}. \end{aligned} \quad (5)$$

This field is a periodic function of  $x_1$  with period  $a$ . Therefore, its Fourier expansion contains only wave vectors  $k_{1n} = nQ$  ( $n$  is the order of diffraction). This means that only frequencies  $\omega_n = nvQ$  can be excited. In this case it is more convenient to expand the field over Bloch eigenfunctions of an “empty” wire<sup>18</sup>. These functions are labeled by quasimomentum  $q_1$ ,  $|q_1| \leq Q/2$ , and the band number  $s$ . The expansion includes only  $q_1 = 0$  components and has the form

$$E_1(x_1; t) = \cos \omega t \sum_s E_{[s/2]} u_s(x_1),$$

where

$$u_s(x) = \exp(iQx[s/2](-1)^{s-1})$$

is the  $q_1 = 0^+$  Bloch amplitude  $u_{sq_1}(x)$  within the  $s$ -th band,  $[...]$  is the entire part symbol, and

$$E_n = -E_0 \frac{\pi r_0^2}{ad} nQ d e^{-nQd}. \quad (6)$$

The excited eigenfrequency  $\omega_n = \omega_{[s/2]}$  belongs simultaneously to the top of the lower even band with number  $s = 2n$  and to the bottom of the upper odd band with number  $s = 2n + 1$  (this is the result of  $\mathbf{E}(x)$  parity). Incident field corresponds to  $n = 0$  and we do not take it into account.

Turning to  $\mathbf{q}, s$  representation with the help of the expansion

$$\begin{aligned} \theta_1(x_1, n_2 a) &= \frac{\sqrt{a}}{L} \sum_{\mathbf{sq}} \theta_{1\mathbf{sq}} e^{i(q_1 x_1 + q_2 n_2 a)} \\ &\times \exp(iQx_1[s/2](-1)^{s-1} \text{sign} q_1), \end{aligned} \quad (7)$$

and similarly for  $\theta_2$  and  $\pi_{1,2}$ , one easily sees that only the  $\mathbf{q} = \mathbf{0}$  components are involved in interaction with the incident radiation. The corresponding part of the Hamiltonian (1) has the form (zero quasimomentum index is omitted):

$$\begin{aligned}
H' = & \frac{\hbar}{2} \sum_{j,s} \left( vg\pi_{js}^\dagger \pi_{js} + \frac{\omega_{[s/2]}^2}{vg} \theta_{js}^\dagger \theta_{js} \right) \\
& + \frac{\hbar\phi}{vg} \sum_{ss'} (-1)^{s+s'} \omega_{[s/2]} \omega_{[s'/2]} \left( \theta_{1s}^\dagger \theta_{2s'} + \theta_{2s'}^\dagger \theta_{1s} \right) \\
& - \frac{eL}{\sqrt{2}a} \cos \omega t \sum_s E_{[s/2]} \left( \theta_{1s}^\dagger + \theta_{1s} \right),
\end{aligned}$$

where

$$\phi = \frac{gV_0 r_0^2}{\hbar v a}, \quad \phi \sim 0.007$$

is the dimensionless inter-array interaction. Consider the initial frequency  $\omega$  close to  $\omega_n$ . In a resonant approximation, only four equations of motion for the ‘‘coordinate’’ operators  $\theta_s$  with  $s = 2n, 2n + 1$  are relevant

$$\begin{aligned}
\ddot{\theta}_{1,2n} + \omega_n^2 \theta_{1,2n} + \phi \omega_n^2 (\theta_{2,2n} - \theta_{2,2n+1}) &= L f_n \cos \omega t, \\
\ddot{\theta}_{1,2n+1} + \omega_n^2 \theta_{1,2n+1} - \phi \omega_n^2 (\theta_{2,2n} - \theta_{2,2n+1}) &= L f_n \cos \omega t, \\
\ddot{\theta}_{2,2n} + \omega_n^2 \theta_{2,2n} + \phi \omega_n^2 (\theta_{1,2n} - \theta_{1,2n+1}) &= 0, \\
\ddot{\theta}_{2,2n+1} + \omega_n^2 \theta_{2,2n+1} - \phi \omega_n^2 (\theta_{1,2n} - \theta_{1,2n+1}) &= 0, \quad (8)
\end{aligned}$$

where

$$f_n = \frac{\sqrt{2} v g e}{\hbar \sqrt{a}} E_n.$$

The homogeneous part of this system defines four eigenfrequencies

$$\begin{aligned}
\omega_{gg} = \omega_{ug} = \omega_n, \\
\omega_{uu} \approx \omega_n(1 - \phi), \\
\omega_{gu} \approx \omega_n(1 + \phi).
\end{aligned}$$

The corresponding eigenvectors are symmetrized combinations of the four operators which enter Eq.(8). They have a fixed parity with respect to permutation of arrays (the first index) and neighboring bands (the second index). Only two modes (even with respect to band index)

$$\begin{aligned}
\theta_{gg} &= \frac{1}{2} (\theta_{1,2n} + \theta_{1,2n+1} + \theta_{2,2n} + \theta_{2,2n+1}), \\
\theta_{ug} &= \frac{1}{2} (\theta_{1,2n} + \theta_{1,2n+1} - \theta_{2,2n} - \theta_{2,2n+1})
\end{aligned}$$

interact with an external field. Therefore only the unperturbed frequency  $\omega_n = \omega_{gg} = \omega_{ug}$  will be absorbed. The two equations of motion for the operators  $\theta_{gg,ug}$  have the same form

$$\ddot{\theta}_\alpha + 2\gamma \dot{\theta}_\alpha + \omega_n^2 \theta_\alpha = L f_n \cos \omega t,$$

where  $\alpha = gg, ug$ . Employing standard procedure in the vicinity of the resonance  $|\omega - \omega_n| \ll \omega_n$  immediately yields the relative absorption of Lorentz type

$$\begin{aligned}
\frac{\Delta I_n}{I_0} &= 2g \frac{e^2}{\hbar c} \left( \frac{\pi r_0^2}{ad} \right)^2 \\
&\times \frac{\gamma v Q}{(\omega - \omega_n)^2 + \gamma^2} [n Q d e^{-n Q d}]^2, \quad (9)
\end{aligned}$$

where

$$I_0 = \frac{cL^2}{4\pi} E_0^2$$

is the energy of light that falls on the QCB per unit time.

Due to the exponential term in the r.h.s of Eq.(6),  $E_n$  decreases fast with  $n$  and only the first few terms contribute to absorption. The characteristic dimensionless scale of the induced field  $r_0^2/(ad)$  for typical values of QCB parameters equals 0.004. We tabulate below the lowest dimensionless Fourier components of the induced field.

n	1	2	3	4	5
$-\frac{ad}{r_0^2} \frac{E_n}{E_0}$	1.05306	1.12359	0.89914	0.63957	0.42650

The results show that one can hope to probe at least the first five spectral lines corresponding to  $\omega_n$  with  $n = 1, 2, \dots, 5$ .

The width of the absorption line (9) is governed by an attenuation coefficient  $\gamma$ . It was introduced phenomenologically but one can (at least qualitatively) estimate its value. The attenuation is caused by decay of plasmon into phonons. The one phonon decay of the plasmon with wave number  $k$  and frequency  $\omega = v|k|$  into a single phonon with the same  $\omega$  and  $k$  occurs in a single point in 1D and does not yield finite attenuation at all. Multiphonon decay is weak because of the small anharmonic coupling within the wire. As a result, the form of the absorption lines should be determined mainly by the instrumental linewidth.

## B. Scanning of the QCB Spectrum within BZ

Within a geometry considered in the previous subsection, one can probe plasmon spectrum only at the BZ center. To study plasmons with nonzero wave vectors one should add to the system an external diffraction lattice namely a periodic array of metallic stripes parallel to the  $Y$  axis (see Fig.3). The DL plane  $Z = 0$  is parallel to the QCB planes  $Z = -D$  for the upper second array and  $Z = -(D + d)$  for the lower first array (the  $Z$  axis is parallel to the  $x_3$  axis). The distance  $D$  between DL and second array is of the same order that the inter-array distance  $d = 2$  nm. The angle between DL wires and the *second* array is  $\varphi$  ( $0 < \varphi < \pi/2$ ). To get a wave number  $K$  of a diffraction field much smaller than  $Q$  one needs a DL with a period  $A$  much larger than the QCB period  $a$ . In the following numerical estimations we choose  $A \approx 200$  nm.

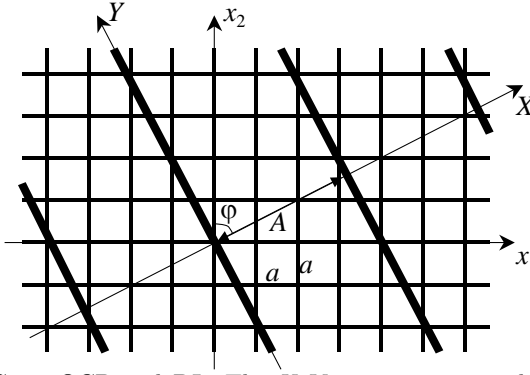


FIG. 3. QCB and DL. The  $X, Y$  axes are oriented along the DL stripes and the wave vector  $\mathbf{K}$  of the diffraction field respectively. The DL (QCB) period is  $A$  ( $a$ ).

Consider an incident field with electric vector  $\mathbf{E} = E_0 \mathbf{e}_X \cos(\mathbf{k}\mathbf{r} - \omega t)$  oriented along the  $X$  axis (perpendicular to the DL wires). The radius  $R_0$  of a DL wire is assumed to be not much larger than the nanotube radius  $r_0$ . In this case light scattering on the DL is similar to that considered in subsection III A). Then the diffraction field is concentrated along the  $X$  direction and has the form (compare with Eq.(5))

$$E_X(X, Z, t) = -E_0 \cos \omega t \times \sum_N \frac{R_0^2 (Z^2 - (X - NA)^2)}{(Z^2 + (X - NA)^2)}.$$

The Fourier transform of the diffraction field is

$$E_X(\mathbf{K}, Z) = -E_0 \frac{\pi R_0^2}{A|Z|} |KZ| e^{-|KZ|},$$

where

$$\mathbf{K}(M) = K \mathbf{e}_X = (K_1, K_2) = \frac{2\pi M}{A} (\sin \varphi, \cos \varphi)$$

with positive integer  $M$ . This means that all the points  $\mathbf{K}$  lie on the same ray oriented along the positive direction of the  $X$  axis. The vector  $\mathbf{K}(M)$  for a fixed  $M$  can be uniquely represented as a sum of quasimomenta lying in the first BZ and two reciprocal lattice vectors

$$\mathbf{K}(M) = \mathbf{q}(M) + \mathbf{m}_1(M) + \mathbf{m}_2(M).$$

The field components

$$\begin{aligned} E_{1\mathbf{K}} &= E_X(\mathbf{K}, D + d) \sin \varphi, \\ E_{2\mathbf{K}} &= E_X(\mathbf{K}, D) \cos \varphi \end{aligned} \quad (10)$$

parallel to the quantum wires, can excite plasmons and contribute to the absorption process.

The Hamiltonian (1) of QCB interacting with an external field in Fourier

$$\begin{aligned} H_j &= \frac{\hbar}{2} \sum_{\mathbf{q}\mathbf{m}_j} \left\{ vg \pi_{j\mathbf{q}+\mathbf{m}_j}^\dagger \pi_{j\mathbf{q}+\mathbf{m}_j} + \right. \\ &\quad \left. + \frac{\omega_{q_j+m_j}^2}{vg} Q_{j,\mathbf{q}+\mathbf{m}_j}^\dagger \theta_{j,\mathbf{q}+\mathbf{m}_j} \right\}, \quad j = 1, 2, \end{aligned} \quad (11)$$

$$H_{12} = \frac{\hbar}{vg} \sum_{\mathbf{m}, \mathbf{q}} \Phi_{\mathbf{q}+\mathbf{m}} \theta_{1,\mathbf{q}+\mathbf{m}_1}^\dagger \theta_{2,\mathbf{q}+\mathbf{m}_2}, \quad (12)$$

$$\begin{aligned} H_E &= \frac{\hbar L}{2vg} \sum_{\mathbf{K}} \left[ f_{1,\mathbf{K}} \left( \theta_{1,\mathbf{K}} + \theta_{1,\mathbf{K}}^\dagger \right) + \right. \\ &\quad \left. + f_{2,\mathbf{K}} \left( \theta_{2,\mathbf{K}} + \theta_{2,\mathbf{K}}^\dagger \right) \right], \end{aligned}$$

where

$$\begin{aligned} \Phi_{\mathbf{K}} &= \phi \xi_{k_1} \xi_{k_2}, \quad \xi_k = \omega_k \text{sign} k, \quad \omega_k = v|k|, \\ f_{j,\mathbf{K}} &= \frac{\sqrt{2} v g e}{\hbar \sqrt{a}} E_{j,\mathbf{K}}, \quad \mathbf{m} = \mathbf{m}_1 + \mathbf{m}_2. \end{aligned} \quad (13)$$

In this subsection we are interested not in the form of the absorption line but only in the resonant frequencies. Therefore, we did not introduce any phenomenological attenuation. The equations of motion for boson fields have the form

$$\begin{aligned} \ddot{\theta}_{1,\mathbf{q}+\mathbf{m}_1} + \omega_{q_1+m_1}^2 \theta_{1,\mathbf{q}+\mathbf{m}_1} + \sum_{m_2} \Phi_{\mathbf{q}+\mathbf{m}} \theta_{2,\mathbf{q}+\mathbf{m}_2} &= L \sum_{M,m_2} f_{1,\mathbf{K}} \delta_{\mathbf{K},\mathbf{q}+\mathbf{m}}, \\ \ddot{\theta}_{2,\mathbf{q}+\mathbf{m}_2} + \omega_{q_2+m_2}^2 \theta_{2,\mathbf{q}+\mathbf{m}_2} + \sum_{m_1} \Phi_{\mathbf{q}+\mathbf{m}} \theta_{1,\mathbf{q}+\mathbf{m}_1} &= L \sum_{M,m_1} f_{2,\mathbf{K}} \delta_{\mathbf{K},\mathbf{q}+\mathbf{m}}. \end{aligned} \quad (14)$$

Only the first few terms in the sum over  $K$  in the r.h.s. of Eq. (14) really excite the QCB plasmons. Indeed, the diffraction field (7) is proportional to the same dimensionless function of the type  $te^{-t}$  ( $t = |KZ_j|$ ) as in the previous subsection (see Eq.(6)). This function has its maximum at  $t = 1$  and differs significantly from zero for  $0.2 < t < 2.7$ . For  $a = 20$  nm,  $D = 2$  nm, it is of order unity within the interval  $0.18Q < |K| < 2.13Q$  for the first array ( $Z_1 = D + d$ ), and within the interval  $0.36Q < |K| < 4.26Q$  for the second array ( $Z_1 = D$ ). This means that one can excite the modes of four lower bands ( $K < 2Q$ ) of the first array and the modes of eighth lower bands ( $K < 4Q$ ) of the second array.

According to Eqs. (10) the field  $E_{j\mathbf{K}(M)}$  is coupled with plasmons of wave vectors  $\mathbf{q} + \mathbf{m}_j = \mathbf{q}(M) + \mathbf{m}_j(M)$  within the  $j$ -th array. The nature of the excited plasmons as well as their frequencies depend on the direction of the vector  $\mathbf{K}(M)$ . For simplicity we restrict ourselves by acute angles  $0 < \varphi < \pi/2$  describing orientation of both DL and vector  $\mathbf{K}(M)$ . There are four kinds of dimensional crossover depending on specific directions in the BZ. Each type of crossover is characterized by its own set of absorption lines. The first one takes place in a common case when  $\mathbf{K}(M)$  for any  $M$  never reaches neither a resonant direction nor the BZ boundary. The second case corresponds to the bisectorial direction  $\varphi = \pi/4$  where the main resonant condition  $\omega(K_1) = \omega(K_2)$  is fulfilled. The third group of directions is determined by another resonant condition  $\omega(K_1) = \omega(nQ \mp K_2)$ . Finally, the fourth group is formed by directions intersecting with the BZ boundaries for some values of  $M$ . In what follows

we consider these four cases separately.

1. In the general case, the points  $\mathbf{K}(M)$  for all  $M$  are far from the BZ diagonals and boundaries. Therefore each of them corresponds to two plasmons mostly propagating along the  $j$ -th array,  $j = 1, 2$ , with unperturbed frequencies  $\omega_{K_j(M)} = vK_j(M)$ . The inter-array interaction slightly renormalizes the eigenfrequencies

$$\begin{aligned}\omega_{1\mathbf{K}}^2 &= \omega_{K_1}^2 + \phi^2 \sum_{m_2} \frac{\omega_{K_1}^2 \omega_{K_2+m_2Q}^2}{\omega_{K_1}^2 - \omega_{K_2+m_2Q}^2}, \\ \omega_{2\mathbf{K}}^2 &= \omega_{K_2}^2 + \phi^2 \sum_{m_1} \frac{\omega_{K_2}^2 \omega_{K_1+m_1Q}^2}{\omega_{K_2}^2 - \omega_{K_1+m_1Q}^2}.\end{aligned}$$

Thus, increasing the frequency of an incident light one observes a set of single absorption lines that consists of two almost equidistant subsets with frequencies corresponding to excitation of plasmons in the first or second arrays. The distances between adjacent lines within each subset are

$$\begin{aligned}\Delta\omega_1 &= v\Delta K_1 = 2\pi v \sin \varphi/A, \\ \Delta\omega_2 &= v\Delta K_2 = 2\pi v \cos \varphi/A,\end{aligned}$$

and their ratio depends on the DL orientation  $\varphi$  only

$$\frac{\Delta\omega_1}{\Delta\omega_2} = \tan \varphi.$$

2. In the resonant case  $\varphi = \pi/4$ , the relation  $K_1(M) = K_2(M)$  is satisfied for all  $M$ . Therefore modes propagating along the two arrays are always degenerate. Inter-array interaction lifts the degeneracy. Indeed, in the resonant approximation, the coupled equations of motion for the field operators read

$$\begin{aligned}\ddot{\theta}_{1\mathbf{K}} + \omega_{K_1}^2 \theta_{1\mathbf{K}} + \phi \omega_{K_1}^2 \theta_{2\mathbf{K}} &= f_{1\mathbf{K}}, \\ \ddot{\theta}_{2\mathbf{K}} + \omega_{K_1}^2 \theta_{2\mathbf{K}} + \phi \omega_{K_1}^2 \theta_{1\mathbf{K}} &= f_{2\mathbf{K}}.\end{aligned}$$

After symmetrization  $\theta_{g,u} = (\theta_{1\mathbf{K}} \pm \theta_{2\mathbf{K}})/\sqrt{2}$ , they have the same form

$$\ddot{\theta}_\alpha + \omega_\alpha^2 \theta_\alpha = f_\alpha,$$

where

$$\omega_{g,u} = \omega_K \left( 1 \pm \frac{1}{2} \phi \right)$$

are the renormalized frequencies,  $\alpha = g, u$ , and  $f_{g,u} = (f_{1\mathbf{K}} \pm f_{2\mathbf{K}})/\sqrt{2}$ . The amplitudes  $f_{g,u}$  are of the same order of magnitude because the distances  $D$  and  $d$  are different but have the same order of magnitude. As a result, increasing the frequency of an incident light one observes an equidistant set of absorption doublets with distance  $\pi\sqrt{2}v/A$  between adjacent doublets.

3. Consider now the directions  $\varphi$  determined by the equation

$$\sin \left( \varphi \pm \frac{\pi}{4} \right) = \frac{nA}{\sqrt{2}M_0a},$$

where  $n$  and  $M_0$  are mutually prime integers. For this direction, two components of the first  $M_0 - 1$  points  $\mathbf{K}(M)$  do not satisfy any resonant condition while the  $M_0$ -th one does

$$K_1(M_0) \pm K_2(M_0) = nQ. \quad (15)$$

With increasing  $M$  this situation is reproduced periodically so that all points  $\mathbf{K}(pM_0)$  with  $p$  integer satisfy a similar condition with  $pn$  standing instead of  $n$ , while all intermediate points are out of resonance.

In the zero approximation with respect to the inter-array interaction we expect to observe two set of absorption lines with frequencies  $p\omega_j = vK_j(pM_0)$ ,  $j = 1, 2$ , corresponding to excitation of plasmons within the  $pm_j(M_0)$ -th band of the  $j$ -th array. The ratio of the frequencies  $\omega_j$  is defined by DL orientation

$$\frac{\omega_1}{\omega_2} = \tan \varphi.$$

However, due to the resonance condition (15), plasmon in the first array with wave vector  $K_1(pM_0)$  and frequency  $\omega_1 = vK_1(pM_0)$  is coupled with plasmon in the second array with the same frequency and wave vector  $K'_2 = \mp(npQ - K_1(pM_0))$  (inter-array degeneracy). Similarly, plasmon in the second array with wave vector  $K_2(pM_0)$  and frequency  $\omega_2 = vK_2(pM_0)$  is coupled with plasmon in the first array with the same frequency and wave vector  $K'_1 = npQ \mp K_2(pM_0)$ . This degeneracy of two modes corresponding to the same band but to different arrays is lifted by the inter-array interaction. As a result one has two sets of doublets instead of two sets of single lines.

Thus, for such orientation of DL, increasing frequency of an incident wave one should observe two equidistant sets of single absorption lines with two sets of equidistant doublets built in these series

$$\begin{aligned}\omega_{1\mathbf{K}} &= \omega_{K_1(pM_0)} \left( 1 \pm \frac{1}{2} \phi \right), \\ \omega_{2\mathbf{K}} &= \omega_{K_2(pM_0)} \left( 1 \pm \frac{1}{2} \phi \right).\end{aligned}$$

In the case  $n = 1$  the lower doublet lies in the first energy band, whereas the upper one lies in the second band. For  $A/a = 10$  (that corresponds to the realistic values of the parameters  $a = 20$  nm and  $A = 200$  nm) the lowest doublet ( $p = 1$ ) will be observed for example for integer  $M_0 = 8$ , at the angle  $\varphi(8) \approx 17^\circ$ , around frequencies  $\omega_1(8) = 0.76vQ$ ,  $\omega_2(8) = 0.24vQ$ .

4. It seems that a similar behavior will be manifested in the case when the points  $\mathbf{K}_{pM}$  lie at one of the BZ boundaries, i.e. satisfy the relation

$$K_j(pM_j) = \frac{npQ}{2}$$

with some specific values  $j$ ,  $M_j$  and  $n$ . Such situation is realized at specific angles that depend on the integers  $j, n, M_j$ . In the vicinity of the points  $\mathbf{K}(pM_j)$  two frequencies corresponding to the unperturbed modes of the  $j$ -th array from the  $np$ -th and  $(np + 1)$ -th bands coincide. This is the case of inter-band degeneracy that is also lifted by inter-array interaction. Due to the square symmetry (invariance with respect to  $x_j \rightarrow -x_j$  inversion), only one of the two components with frequency  $\omega = v|K_j(pM_j)|$  may be excited by a diffraction field. Therefore, this case does not differ from the case **1** considered above and two sets of equidistant single lines can be observed.

We emphasize that studying absorption of light by QCB one can expose, beyond the standard<sup>18</sup> dimensional crossover with respect to an angle (direction), also occurrence of a new type of crossover with *an external frequency* as a control parameter. This occurs for special directions of type **3** where, with increasing frequency, the set of single lines is periodically intermitted by doublets.

#### IV. QCB ON A SEMICONDUCTING SUBSTRATE

##### A. Hamiltonian

An alternative method of examination of the plasmon spectrum in QCB is the study of its interaction with the substrate, whose electrodynamic properties are well known. An excellent material for this purpose is a III-V semiconductor. Surface plasmons in semiconductor slab can be excited in a controllable way (see Refs.<sup>21,22</sup> and literature therein), and these plasmons can be in resonance with Bose excitations in QCB.

In this section we consider dielectric properties of QCB placed on a semiconducting substrate (Fig.1). Any surface wave excited in the substrate is coupled with QCB-plasmon modes due to the substrate-QCB interaction. Such an interaction gives an opportunity to probe QCB spectrum via IR absorption of the substrate (see below). Assuming the distance  $D$  between the first array and the substrate to be much smaller than the distance  $d$  between arrays, one can keep only the interaction between the substrate and the first array. In this case the system is described by the Hamiltonian

$$H = H_0 + H_{int}. \quad (16)$$

Its unperturbed part

$$H_0 = H_K + H_1 + H_2$$

contains the Hamiltonians (11) of the two arrays and the kinetic energy of the substrate electrons with effective mass  $m$  and quadratic dispersion law  $\varepsilon_{\mathbf{k}} = \frac{\hbar^2 k^2}{2m}$  (we omit the irrelevant spin variables)

$$H_K = \sum_{\mathbf{q}\mathbf{m}} \varepsilon_{\mathbf{q}+\mathbf{m}} c_{\mathbf{q}+\mathbf{m}}^\dagger c_{\mathbf{q}+\mathbf{m}}.$$

Here as in the previous section, a quasi wave vector  $\mathbf{q}$  belongs to the first BZ and  $\mathbf{m}$  is a reciprocal lattice vector. The interaction part of the Hamiltonian (16)

$$H_{int} = H_C + H_{s1} + H_{12}.$$

includes inter-array interaction (12), Coulomb interaction within the substrate

$$H_C = \frac{1}{2} \sum_{\mathbf{q}\mathbf{m}} U_{\mathbf{q}+\mathbf{m}} \rho_{\mathbf{q}+\mathbf{m}}^\dagger \rho_{\mathbf{q}+\mathbf{m}},$$

$$\rho_{\mathbf{k}} = \frac{1}{L} \sum_{\mathbf{k}'} c_{\mathbf{k}'}^\dagger c_{\mathbf{k}+\mathbf{k}'}, \quad U_{\mathbf{k}} = \frac{2\pi e^2}{k}, \quad \mathbf{k} = \mathbf{q} + \mathbf{m}$$

and an interaction  $H_{s1}$  between the substrate and the first array. The latter interaction is a capacitive coupling between charge fluctuations in the substrate and collective modes in the nearest array. In coordinate representation it is written as

$$H_{s1} = \sum_{n_2} \int dx_1 dx_1' dx_2 W(x_1 - x_1', x_2 - n_2 a) \times \\ \times \rho(x_1, x_2) \partial_{x_1'} \theta_1(x_1', n_2 a).$$

Here  $\rho(\mathbf{r})$  is the density operator for the substrate electrons,  $\sqrt{2} \partial_{x_1'} \theta_1(x_1', n_2 a)$  is the density operator of the first array, and  $W(\mathbf{r} - \mathbf{r}')$  is Coulomb interaction between the substrate and array

$$W(\mathbf{r}) = \frac{\sqrt{2} e^2 \zeta \left( \frac{x_1}{r_0} \right)}{\sqrt{|\mathbf{r}|^2 + D^2}}.$$

In momentum representation the interaction between the substrate and the array has the form:

$$H_{s1} = \sqrt{\frac{\hbar}{vg}} \sum_{\mathbf{m}\mathbf{q}} W_{\mathbf{q}+\mathbf{m}} \rho_{\mathbf{q}+\mathbf{m}} \theta_{1,\mathbf{q}+\mathbf{m}}^\dagger, \quad (17)$$

where

$$W_{\mathbf{k}} = ik_1 \sqrt{\frac{vg}{\hbar a}} \int dx_1 dx_2 W(\mathbf{r}) e^{i\mathbf{k}\mathbf{r}}$$

is proportional to the Fourier component of  $W(\mathbf{r})$ .

##### B. Dielectric Function

The high frequency properties of the system at zero temperature are determined by the zeroes of the dielectric function

$$\frac{1}{\varepsilon(\mathbf{k}, \omega)} = 1 + U_{\mathbf{k}} \Pi(\mathbf{k}, \omega). \quad (18)$$

Here



$$\Pi(\mathbf{k}, \omega) = -\frac{i}{\hbar} \int_0^\infty dt e^{i\omega t} \left\langle \left[ \rho_{\mathbf{k}}(t), \rho_{\mathbf{k}}^\dagger(0) \right] \right\rangle, \quad (19)$$

is the polarization of the *substrate interacting with QCB*,  $\rho_{\mathbf{k}}(t) = e^{iHt/\hbar} \rho_{\mathbf{k}} e^{-iHt/\hbar}$  is the density of the *substrate* electrons in the Heisenberg representation, and averaging is performed over the ground state of the Hamiltonian (16).

Dielectric properties of the substrate *per se* within the RPA approach are described by the 2D version of the Lindhard formula

$$\begin{aligned} \epsilon_s(\mathbf{k}, \omega) &= 1 - U_{\mathbf{k}} \Pi_0(\mathbf{k}, \omega), \\ \Pi_0(\mathbf{k}, \omega) &= \frac{1}{L^2} \sum_{\mathbf{k}'} \frac{\theta(\epsilon_F - \epsilon_{\mathbf{k}'}) - \theta(\epsilon_F - \epsilon_{\mathbf{k}+\mathbf{k}'})}{\hbar\omega - (\epsilon_{\mathbf{k}+\mathbf{k}'} - \epsilon_{\mathbf{k}'}) + i0}. \end{aligned} \quad (20)$$

The *substrate* polarization  $\Pi_s(\mathbf{k}, \omega)$  is defined by the same Eq.(19) where the averaging in the r.h.s. is performed with respect to the *substrate* Hamiltonian  $H_s = H_K + H_C$ . It can be written as

$$(\Pi_s(\mathbf{k}, \omega))^{-1} = (\Pi_0(\mathbf{k}, \omega))^{-1} - U_{\mathbf{k}}, \quad (21)$$

that results in the expression for the dielectric function

$$\frac{1}{\epsilon_s(\mathbf{k}, \omega)} = 1 + U_{\mathbf{k}} \Pi_s(\mathbf{k}, \omega) \quad (22)$$

similar to Eq.(18).

The active branches of substrate excitations are the surface density fluctuations which consist of 2D electron-hole pairs and surface plasmon mode with dispersion law

$$\omega_s(k) = v_F k \sqrt{1 + \frac{1}{2kr_B}}, \quad (23)$$

where  $r_B = \frac{\hbar^2}{m_e^2}$  (see e.g. Ref. 23). The RPA spectrum of surface excitations is shown in Fig.4.

For GaAs, the substrate parameters are  $m = 0.068m_0$ ,  $m_0 = 9.1 \cdot 10^{-28}$  g is the mass of a free electron,  $v_F = 8.2 \cdot 10^6$  cm/sec,  $r_B = 0.78$  nm,  $\omega_0 = v_F/r_B = 1.05 \times 10^{14}$  sec<sup>-1</sup>. For  $k < k^* \approx 0.1r_B^{-1}$ , the plasmon frequency lies above the continuum spectrum of electron-hole pairs and the substrate plasmons are stable. Besides, one may easily satisfy the resonance condition for the collective plasmon mode near the stability threshold  $k \sim k^*$  and QCB excitations with frequency  $\sim 10^{14}$  sec<sup>-1</sup>. For large enough  $k > k^*$  the plasmon dispersion curve lies within the quasi-continuum spectrum and plasmons become unstable with respect to decay into electron-hole pairs (Landau damping of the substrate plasmons).

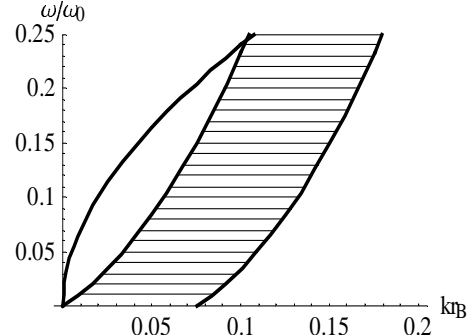


FIG. 4. Dispersion of the substrate plasmons (upper line) and quasi-continuum spectrum of electron-hole excitations, (dashed area). Frequency is measured in  $\omega_0 = v_F/r_B$  units.

To obtain the dielectric function of the whole system substrate plus QCB (18), one should take into account that Umklapp processes stimulated by interaction between the substrate and the first array (17) as well as the interaction between arrays (12), produce modes with wave vectors  $\mathbf{q} + \mathbf{m}$  with various reciprocal lattice vectors  $\mathbf{m}$ . This necessarily leads to appearance of non-diagonal components of the polarization operator

$$\Pi(\mathbf{q} + \mathbf{m}, \mathbf{q} + \mathbf{m}'; \omega) = -\frac{i}{\hbar} \int_0^\infty dt e^{i\omega t} \left\langle \left[ \rho_{\mathbf{q}+\mathbf{m}}(t), \rho_{\mathbf{q}+\mathbf{m}'}^\dagger(0) \right] \right\rangle.$$

In what follows we always consider a fixed frequency  $\omega$  and a fixed wave vector  $\mathbf{q}$  in the BZ. Henceforth the variables  $\mathbf{q}$  and  $\omega$  are omitted below for simplicity. In the framework of RPA approach,  $\Pi(\mathbf{m}, \mathbf{m}')$  satisfies the following Dyson-type equation

$$\text{Diagram}(\mathbf{m}, \mathbf{m}') = \text{Diagram}(\mathbf{m}) \delta_{\mathbf{m}\mathbf{m}'} + \text{Diagram}(\mathbf{m}, \mathbf{m}') \quad (24)$$

Here the first term  $\text{Diagram}(\mathbf{m}) = \Pi_s(\mathbf{m})$  in the right hand side is the substrate polarization (21) of the isolated substrate itself, the empty point  $\mathbf{m} = W_{\mathbf{m}} \equiv W_{\mathbf{q}+\mathbf{m}}$  is a simple vertex which describes substrate - (first) array interaction, and the thick line

$$\text{Diagram}(\mathbf{m}_j, \mathbf{m}') = -\frac{i}{\hbar} \int_0^\infty dt e^{i\omega t} \left\langle \left[ \theta_{j\mathbf{q}+\mathbf{m}_j}(t), \rho_{\mathbf{q}+\mathbf{m}'}^\dagger(0) \right] \right\rangle \quad (25)$$

is the correlation function of the  $j$ -th array mode and the substrate plasmon.

The Dyson equation (24) should be completed by two equations for the correlation functions (25) ( $j = 1, 2$ )

$$\text{Diagram}(\mathbf{m}_1, \mathbf{m}') = \text{Diagram}(\mathbf{m}_2) \text{Diagram}(\mathbf{m}_1, \mathbf{m}') + \text{Diagram}(\mathbf{m}_1, \mathbf{m}') \quad (26)$$

$$\text{Diagram}(\mathbf{m}_2, \mathbf{m}') = \text{Diagram}(\mathbf{m}_1, \mathbf{m}') \quad (27)$$

Here the dashed line  $\text{Diagram}(\mathbf{m}_j) = D_j^0(m_j)$  ( $j = 1, 2$ ) is the bare correlation function of the  $j$ -th array modes

$$D_j^0(m_j) = -\frac{i}{vg} \int_0^\infty dt e^{i\omega t} \left\langle \left[ \theta_{j\mathbf{q}+\mathbf{m}_j}(t), \theta_{j\mathbf{q}+\mathbf{m}_j}^\dagger(0) \right] \right\rangle_0$$

$$= \frac{1}{\omega^2 - v^2(q_j + m_j)^2},$$

and two triangles  $\Delta^{\frac{m_1}{m_2}} = \sqrt{\hbar\phi/vg\xi_{q_1+m_1Q}}$  and  $\nabla^{\frac{m_2}{m_1}} = \sqrt{\hbar\phi/vg\xi_{q_2+m_2Q}}$  form the second vertex describing the separable inter-array interaction (13).

Solving the system of equations (24), (26) and (27) one obtains the diagonal element  $\Pi(\mathbf{m}) \equiv \Pi(\mathbf{m}, \mathbf{m})$  of the polarization operator

$$[\Pi(\mathbf{m})]^{-1} = [\Pi_s(\mathbf{m})]^{-1} - |W_{\mathbf{m}}|^2 D(\mathbf{m}). \quad (28)$$

The second term in the right-hand side of this equation describes renormalization of this vertex by interaction between the substrate and QCB. The factor  $D(\mathbf{m})$  is a renormalized correlation function of modes of the first array

$$[D(\mathbf{m})]^{-1} = [D_1^0(m_1)]^{-1} - (w(\mathbf{m}) + \varphi(m_1)). \quad (29)$$

Here  $w(\mathbf{m})$  describes the effective interaction between the first array and substrate

$$w(\mathbf{m}) = F(m_1) - |W_{\mathbf{m}}|^2 \Pi_s(\mathbf{m}),$$

$$F(m_1) = \sum_{m_2} |W_{\mathbf{m}}|^2 \Pi_s(\mathbf{m}) \quad (30)$$

and  $\varphi(m_1)$  is the effective interaction between the two arrays

$$\frac{\omega_{m_1}^2}{\varphi(m_1)} = \left[ \phi^2 \sum_{m_2} \omega_{m_2}^2 D_2^0(m_2) \right]^{-1} - \Psi_{m_1}, \quad (31)$$

$$\omega_{m_j} = v(q_j + m_j Q),$$

renormalized by Coulomb interaction of array modes with substrate plasmons,

$$\Psi_{m_1} = \sum_{m'_1 \neq m_1} \frac{\omega_{m'_1}^2}{(D_1^0(m'_1))^{-1} - F(m'_1)}. \quad (32)$$

Equations (28) - (32) together with the definition (18) solve the problem of dielectric properties of the combined system QCB-substrate within RPA.

The whole  $\{\omega, \mathbf{k}\}$  space can be divided into two parts. Within the first subspace the dielectric function (18) is a real function. Its zeros define the spectrum of collective modes. Within the second subspace the dielectric function has non-zero imaginary part. The latter is related to regions where these excitations are unstable. These two subspaces will be considered separately in the next two subsections.

## C. Excitations

The spectrum of collective excitations in QCB-substrate system is determined by zeroes of the dielectric function  $\epsilon(\mathbf{q}, \omega) = 0$ . In the low frequency limit  $\omega \ll vQ/2$  taking into account only contribution of the lowest QCB band (i.e. omitting the terms with  $\mathbf{m}' \neq 0$ ), we obtain the dispersion equation

$$(\omega^2 - \omega_s^2(q)) \left[ (\omega^2 - (1-\alpha)v^2q_1^2) (\omega^2 - (1-\alpha)v^2q_2^2) - \phi^2 \xi_{q_1}^2 \xi_{q_2}^2 \right] - \frac{2m}{\pi^2 \hbar^2} v_F^2 q^2 |W_{\mathbf{q}}|^2 (\omega^2 - v^2q_2^2) = 0, \quad (33)$$

$$\alpha = \phi^2 \frac{a}{r_0},$$

where  $\omega_s(q)$  is the substrate plasmon frequency (23). Neglecting both inter-array ( $\propto \phi^2$ ) and substrate-first array ( $\propto W_{\mathbf{q}}^2$ ) interactions, we are left with the substrate plasmon mode and the modes of two arrays. Asymmetry of the dispersion relation (33) with respect to the two QCB arrays reflects the fact that the substrate interacts only with the first array.

The key question is the robustness of the QCB spectrum against interaction with 2D substrate excitations. To answer this question we note that for wave vector  $\mathbf{q} \rightarrow 0$  both interactions vanish

$$\xi_{q_1}^2 \xi_{q_2}^2 |W_{\mathbf{q}}|^2 \rightarrow 0 \quad (34)$$

for all directions of  $\mathbf{q}$  except the first array direction  $x_1$  (the latter direction is singular in all similar 1D - 2D problems). Therefore in the long wave limit  $q \ll Q$  the interaction just renormalizes the bare dispersion laws of the arrays

$$\frac{\omega_j^2}{v^2 q_j^2} = 1 - \alpha - \delta_{1j} \alpha_{\mathbf{q}}, \quad \alpha_{\mathbf{q}} = \frac{1}{2\pi v^2 e^2} \frac{q |W_{\mathbf{q}}|^2}{q_1^2},$$

conserving its LL linearity. This result verifies stability of QCB plasmons with respect to substrate-QCB interaction.

The dispersion relation (33) shows that the QCB-substrate interaction results in appearance of two more resonant directions in the BZ. In addition to the diagonal line  $OJ$  (Fig.5) that is the resonance line for inter-array interaction, two new lines arise, which correspond to resonant interaction of the substrate with the first or the second array. The resonance condition  $\omega_s(q) = vq_j \equiv \omega_j(\mathbf{q})$  is fulfilled along the line  $LN$  for  $j = 1$  and along the line  $KM$  for  $j = 2$ . The points  $J, M$  on these lines are the points of onset of Landau damping. The region of Landau damping exists outside the curve  $WJUMR$  and consists of two subregions. One of them exists in an isolated substrate outside the arc  $PNUMR$ . Another region is secluded within the close curve  $WJUNPW$  and appears exclusively due to QCB-substrate interaction (see subsection IV D for details).

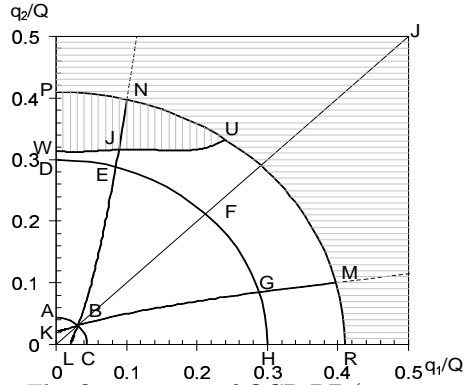


FIG. 5. The first quarter of QCB BZ ( $a = 20$  nm). QCB plasmons are in resonance with surface plasmons along the lines  $OM$  and  $ON$ . The surface plasmons are stable within the internal part of BZ bounded by the curve  $WJU$  and the arc  $UMR$ .

Far from the symmetric point  $B$ , the two renormalized dispersion laws along  $LN$  are

$$\omega_{\pm}^2 = v^2 q_1^2 (1 \pm \sqrt{\alpha_{\mathbf{q}}}). \quad (35)$$

They describe the splitting of two coupled substrate-first array modes. The third mode is slightly renormalized plasmon propagating along the second array. Along the resonance line  $KM$  one of the dispersion laws conserves its bare form

$$\omega = vq_2$$

while another one transforms into

$$\frac{\omega^2}{v^2 q_2^2} = 1 - (\alpha_{\mathbf{q}} + \alpha) \frac{q_1^2}{q_1^2 - q_2^2}. \quad (36)$$

These two modes are coupled substrate plus second array modes. The third mode represents slightly renormalized plasmon propagating along the first array. Along the diagonal  $OJ$ , the two array modes are in resonance  $vq_1 = vq_2 \equiv \omega(\mathbf{q})$ . Here we get two coupled QCB plasmons with dispersion laws

$$\omega_{\pm} = vq(1 \pm \sqrt{\alpha}) \quad (37)$$

and substrate plasmon with slightly renormalized frequency. At the symmetric point  $B$ ,  $q_{1B} = q_{2B} \approx 0.1Q$ , all three modes are in resonance  $\omega_s(q_B) = vq_{1B} = vq_{2B} \equiv \omega_B$ . Interaction lifts the degeneracy and renormalizes the frequencies

$$\omega_0^2 = \omega_B^2, \quad \omega_{\pm}^2 = \omega_B^2 (1 \pm \sqrt{\alpha_{\mathbf{q}_B} + \alpha}). \quad (38)$$

In Figs. 6, 7 the dispersion curves calculated along the circle arcs with two different radii are shown. Solid lines show the dispersion curves of interacting system whereas the dashed lines describe those of noninteracting substrate and QCB. Here the azimuthal angle  $\varphi$  is introduced as in the previous section.

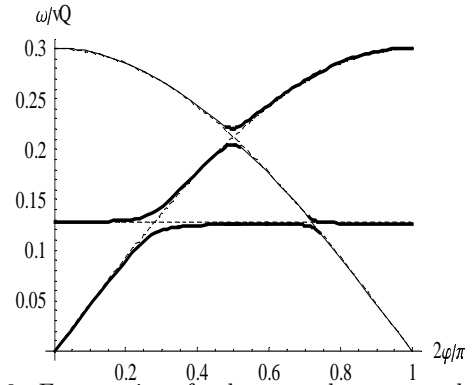


FIG. 6. Frequencies of substrate plasmons and modes of QCB with interaction between them (solid lines) and without the interaction (dashed lines) as functions of the azimuthal angle  $\varphi$  for  $q = 0.3Q$ .

We start with a general case (Fig.6) that represents the dispersion curves along the  $DEFGH$  line for  $q = 0.3Q$ . Points  $D, E, F, G, H$  in Fig.5 correspond to values  $2\varphi/\pi = 0, 0.28, 0.5, 0.72, 1$ . Far from the resonance lines (i.e. not too close to the points  $E, F$  and  $G$ ) the dispersion curves describe slightly renormalized frequencies of the modes propagating within the substrate and along two arrays. At the point  $E$  in Fig. 5, the modes propagating in the substrate and along the first array are degenerate. The substrate-QCB interaction splits this degeneracy and the renormalized frequencies are described by Eq.(35). At the point  $F$ , the modes propagating along the first and second arrays are degenerate and the frequencies are described by Eq.(37). At the point  $G$ , the modes propagating in the substrate and along the second array are degenerate and the frequencies are described by Eq.(36). For any fixed angle  $\varphi$  three absorption lines should exist, but the intensity of that related to the second array is proportional to both (weak) substrate-array and inter-array interaction, so this line is practically not observable. The corresponding dispersion curve is plotted as a thin solid line. On the other hand, the thick solid lines are used for dispersion curves corresponding to the substrate plasmons and excitations of the first array.

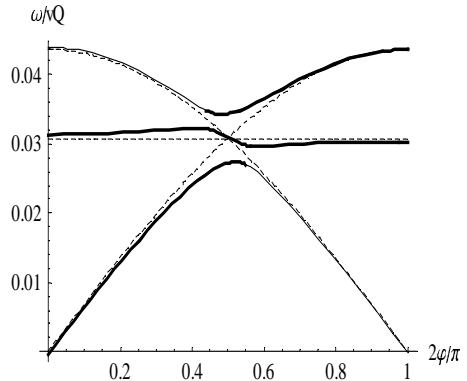


FIG. 7. Frequencies of substrate plasmons and modes of QCB with interaction (solid lines) and without interaction (dashed lines) as functions of azimuthal angle  $\varphi$  for  $q = 0.03Q$ .

Dispersion curves along the line  $ABC$ , ( $\frac{2\varphi}{\pi} =$

0, 0.5, 1.0) that includes the triple resonance point  $B$ , are displayed in Fig.7 (here  $q \approx 0.03Q$ ). Here at point  $B$ , all three modes are strongly coupled and the frequencies are described by Eq.(38). As in the previous figure, dispersion curve corresponding to the second array plasmons is plotted by a thin solid line.

#### D. Landau Damping

Dielectric losses of an isolated substrate are described by an imaginary part of its dielectric function  $\epsilon_s$  (22). This imaginary part is non-zero within the dashed region in Fig.4 due to appearance of imaginary part of the bare polarization operator  $\Pi_0(\mathbf{k}, \omega)$  (20)

$$\Im\Pi_0(\mathbf{k}, \omega) = \frac{m}{2\pi\hbar^2} \frac{1}{\kappa^2} \left[ \theta(\kappa^2 - \nu_+^2) \sqrt{\kappa^2 - \nu_+^2} - \theta(\kappa^2 - \nu_-^2) \sqrt{\kappa^2 - \nu_-^2} \right],$$

$$\kappa = \frac{k}{k_F}, \quad \nu_{\pm} = \nu \pm \frac{\kappa^2}{2}, \quad \nu = \frac{\omega}{v_F k_F}.$$

As was mentioned above, the plasmon dielectric losses are related to the Landau damping of collective excitation with momentum  $k > k^*$ ,  $k^* r_B \approx 0.1$  into electron-hole pair.

The substrate-QCB interaction remarkably changes the conventional picture of substrate plasmon dielectric losses. The imaginary part of the dielectric function  $\epsilon(\mathbf{k}, \omega)$  (18) of the system differs from zero not only within the dashed region. New regions of Landau damping appear due to QCB - substrate interaction. Indeed, QCB serves as a diffraction grid for the substrate like in the case considered in Section III. The corresponding Umklapp processes initiate Landau damping of surface plasmons within the long wave region  $k < k^*$  where the usual Landau damping is absent. The main contribution is related to the renormalization term  $w(\mathbf{m})$  in Eq.(30) due to Umklapp processes along the  $x_2$  axis (summation over  $m_2$  in the expression for function  $F(m_1)$  is implied). It is proportional to the fourth power of QCB - substrate interaction  $W^4$ . The Umklapp processes along both directions  $x_{1,2}$  contribute also to the renormalization term  $\varphi(m_1)$  in Eq.(29). However, they contain additional small parameter  $\phi^4$  related to inter-array interaction within QCB and we do not take them into account.

These new Landau damping regions can be described in detail with the help of a “phase diagram” displayed in Fig.8. Coordinate axes in the figure correspond to the surface plasmon momenta  $k_{1,2}$  along  $x_{1,2}$  directions measured in  $r_B^{-1}$  units. The QCB period is  $a = 30$  nm. Such a choice enables us to realize a rich variety of possible damping scenarios.

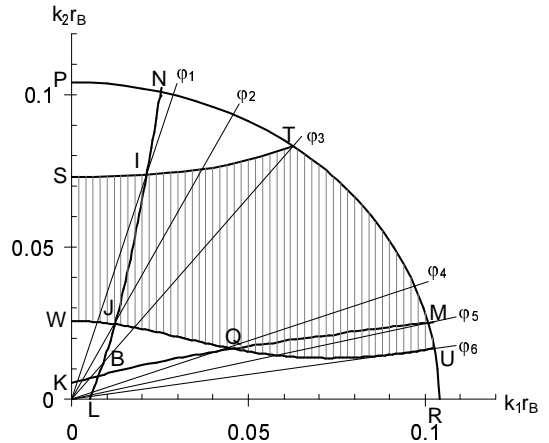


FIG. 8. “Phase diagram” describing possible types of new regions of Landau damping. Superlattice constant is chosen as  $a = 30$  nm. For an isolated substrate Landau damping occurs outside the arc  $PNTMUR$ . New regions are bounded by curves  $SIT$  and  $WJQU$ .

The Landau damping region of the isolated substrate, defined by  $|k| r_B > 0.1$ , is situated outside the circular arc  $PNTMUR$ . A new damping region inside this arc is bounded by two curves  $SIT$  and  $WJQU$ . The line  $LB$  ( $KBQM$ ) corresponds to resonance between substrate plasmon and the first (second) array QCB plasmon. The points  $I, J, T, Q, M, U$  of intersection between the resonant lines, the curves  $SIT$  and  $WJQU$ , and the arc  $PNTMUR$  define six rays  $OI, OJ, OT, OQ, OM$ , and  $OU$  and corresponding six angles  $\varphi_1 = 16^\circ$ ,  $\varphi_2 = 33^\circ$ ,  $\varphi_3 = 38^\circ$ ,  $\varphi_4 = 69^\circ$ ,  $\varphi_5 = 76^\circ$ ,  $\varphi_6 = 81^\circ$ . Each pair of adjacent rays (together with coordinate semiaxes) bounds a specific structure of new damping region.

New damping region corresponding to the substrate plasmon propagating within the first sector  $\varphi < \varphi_1$  is separated quite well from the region of initial Landau damping. In fact it presents a new damping band. Its boundaries are defined by intersection point of the ray with a fixed angle  $\varphi$  with the curves  $SIT$  and  $WJQU$ . The damping amplitude is small because of the small factor of order  $W^4$  mentioned above. When the ray tends to the  $\varphi_1$  direction, small peak appears near the “blue” boundary of the new damping region (precursor of the resonance between the substrate plasmon and the first array QCB plasmon).

Within the second sector  $\varphi_1 < \varphi < \varphi_2$ , well pronounced resonant peak appears within the damping band. It is described in detail in Fig.9 for  $\varphi = 20^\circ$ . The peak amplitude is of the order of damping amplitude within the initial damping region (panel  $a$ ). It has a well pronounced Lorentzian form (panel  $b$ ) placed on the wide and low “pedestal” (panel  $c$ ).

The next two sectors  $\varphi_2 < \varphi < \varphi_3$  and  $\varphi_3 < \varphi < \varphi_4$ , do not contain resonant peaks at all. The new damping region corresponding to the first one of them is still separated from the initial damping region touching it at only at the angle  $\varphi_3$ . For  $\varphi_3 < \varphi < \varphi_4$ , the new damping

band is altered by a weak damping tail. The damping amplitude in the tail is small due to the same reasons mentioned above. It is displayed in the insertion to the Fig.10 for the angle  $\varphi = 68^\circ$ . This angle is close to the sector boundary and a precursor of the resonant peak is well pronounced.

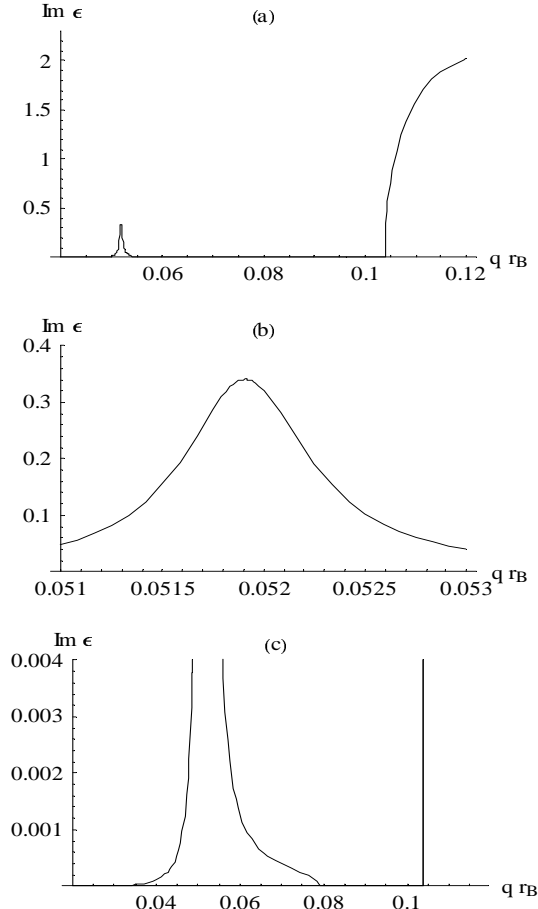


FIG. 9. Additional damping region for  $\varphi = 20^\circ$ . *a)* main peak and initial Landau damping region; *b)* central part of the peak zoomed; *c)* total new damping region and edge of the initial damping region

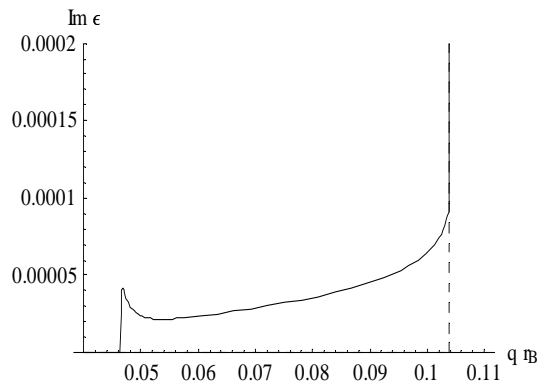


FIG. 10. Damping tail for  $\varphi = 68^\circ$  and the initial damping region. Precursor of the resonant peak is resolved quite well.

Further increase of the angle  $\varphi_4 < \varphi < \varphi_5$  leads to re-appearance of the resonant peak within the tail. In

this case one deals with a resonance between the substrate plasmon and the QCB plasmon in the second array. Existence of this resonance is caused by inter-array interaction that brings additional small parameter to the imaginary part of the dielectric function. As a result, the width of the peak is extremely smaller in the second sector while surprisingly the peak amplitude has the same order of magnitude as in the case of resonance with the nearest to substrate (first) array.

Within the sixth sector  $\varphi_5 < \varphi < \varphi_6$  the damping tail does not contain any resonance. It vanishes at  $\varphi = \varphi_6$  and within the last seventh sector  $\varphi_6 < \varphi < \pi/2$  the damping occurs only within the initial Landau damping band.

The existence of the additional QCB band (tail) of Landau damping and appearance of the resonant peak within the band (tail) is a bright manifestation of interplay between really  $2D$  surface plasmons and quasi- $2D$  QCB plasmons.

## V. CONCLUSION

In conclusion, we investigated the possibility of spectroscopic studies of the excitation spectrum of quantum crossbars, which possesses unique property of dimensional crossover both in spatial coordinates and in  $(\mathbf{q}, \omega)$  coordinates. It follows from our studies that the plasmon excitations in QCB may be involved in resonance diffraction of incident electromagnetic waves and in optical absorption in the IR part of spectrum.

In the case of direct interaction of external electric field with QCB, infrared absorption strongly depends on the direction of the wave vector  $\mathbf{q}$ . One can observe dimensional crossover from  $1D \rightarrow 2D$  behavior of QCB by scanning an incident angle. The crossover manifests itself in the appearance of a set of absorption doublets instead of the set of single lines. At special directions, one can observe new type of crossover where doublets replace the single lines with changing frequency at a fixed  $\mathbf{q}$  direction.

Capacitive contact between QCB and semiconductor substrate does not destroy the LL character of the long wave excitations. However, quite unexpectedly the interaction between the surface plasmons and plasmon-like excitations of QCB essentially influences the dielectric properties of a substrate. First, combined resonances manifest themselves in a complicated absorption spectra. Second, the QCB may be treated as the diffraction grid for a substrate surface, and Umklapp diffraction processes radically change the plasmon dielectric losses. So the surface plasmons are more fragile against interaction with superlattice of quantum wires than the LL plasmons against interaction with  $2D$  electron gas in a substrate.

Dimensional crossover in QCB plays a significant role in all the above phenomena.

### ACKNOWLEDGMENTS

S.G. appreciates discussions with N. Beletskii concerning excitation of surface plasmon in semiconducting substrate. S.G. and I.K. are thankful to V. Liubin and M. Klebanov for discussions of various ways of experimental observation of optical absorption in thin films. This research is partially supported by grants from Israeli Science Foundation and US-Israel Binational Science Foundation.

Dresselhaus, Ph. Avouris (Eds.), Topics Appl. Phys. **80**, 113 (2001), Springer, Berlin 2001.

<sup>21</sup> *Surface Polaritons. Electromagnetic waves at Surfaces and Interfaces*, V.M. Agranovich and D.L. Mills, Eds., Amsterdam, North-Holland, 1982.

<sup>22</sup> *Electromagnetic Surface Modes*, Ed. A.D. Boardman, NY, Wiley, 1982.

<sup>23</sup> F. Stern, Phys.Rev. Lett. **18** 546 (1967).

- 
- <sup>1</sup> M.R. Diehl, S.N. Yaliraki, R.A. Beckman, M. Barahona, and J.R. Heath, Angew. Chem. Int. Ed. **41**, 353 (2002).
- <sup>2</sup> B. Q. Wei, R. Vajtai, Y. Jung, J. Ward, R. Zhang, G. Ramanath, and P. M. Ajayan, Nature **416**, 495 (2002).
- <sup>3</sup> Y. Luo, C. P. Collier, J.O. Jeppesen, K.A. Nielsen, E. Delonno, G. Ho, J. Perkins, H-R. Tseng, T. Yamamoto, J.F. Stoddardt, J.R. Heath, ChemPhysChem **3**, 519 (2002).
- <sup>4</sup> G.V. Tseng, J.C. Ellenbogen, Science **294**, 1293 (2001).
- <sup>5</sup> T. Rueckes, K. Kim, E. Joselevich, G. Y. Tseng, C. L. Cheung, and C. M. Lieber, Science **289**, 94 (2000).
- <sup>6</sup> J.E. Avron, A. Raveh, and B. Zur, Rev. Mod. Phys. **60**, 873 (1988).
- <sup>7</sup> Y. Avishai, J.M. Luck, Phys. Rev. B **45**, 1074 (1992).
- <sup>8</sup> F. Guinea, and G. Zimanyi, Phys. Rev. B **47**, 501 (1993).
- <sup>9</sup> R. Mukhopadhyay, C.L. Kane, and T. C. Lubensky, Phys. Rev. B **63**, 081103(R) (2001).
- <sup>10</sup> M. Bockrath, D.H. Cobden, J. Lu, A.G. Rinzler, R.E. Smalley, L. Balents, P.L. McEuen, Nature **397**, 598 (1999).
- <sup>11</sup> R. Egger, A. Bachtold, M.S. Fuhrer, M. Bockrath, D.H. Cobden, and P.L. McEuen, in *Interacting Electrons in Nanostructures*, p. 125, R. Haug, and H. Schoeller (Eds.), Springer (2001).
- <sup>12</sup> X. G. Wen, Phys. Rev. B **42**, 6623 (1990).
- <sup>13</sup> H. J. Schultz, Int. J. Mod. Phys. **1/2**, 57 (1991).
- <sup>14</sup> I. Kuzmenko, S. Gredeskul, K. Kikoin, and Y. Avishai, Low Temp. Phys. **28**, 539 (2002) [Fiz. Nizk. Temp. **28**,752 (2002)].
- <sup>15</sup> A.H. Castro Neto, and F. Guinea, Phys. Rev. Lett. **80**, 4040 (1998).
- <sup>16</sup> R. Mukhopadhyay, C.L. Kane, and T. C. Lubensky, Phys. Rev. B **64**, 045120 (2001).
- <sup>17</sup> K. Kikoin, I. Kuzmenko, S. Gredeskul, and Y. Avishai, in *Proceedings of NATO Advanced Research Workshop "Recent Trends in Theory of Physical Phenomena in High Magnetic Fields"* (Les Houches, France, February 25 – March 1, 2002); *cond-mat/0205120*.
- <sup>18</sup> I. Kuzmenko, S. Gredeskul, K. Kikoin, and Y. Avishai, Phys. Rev. B **67**, 115331 (2003).
- <sup>19</sup> S. Gredeskul, I. Kuzmenko, K. Kikoin, and Y. Avishai, Physica E **17**, 187 (2003).
- <sup>20</sup> S.G. Louie in *Carbon Nanotubes*, M.S. Dresselhaus, G.

**m**  
•